Heteromultivalency enables enhanced detection of nucleic acid mutations

Brendan R. Deal, Rong Ma, Hiroaki Ogasawara, James T. Kindt, and Khalid Salaita*

Department of Chemistry, Emory University, Atlanta, Georgia 30322, United States

*Correspondence should be addressed to K.S. (email: k.salaita@emory.edu)

Abstract

Detecting genetic mutations such as single nucleotide polymorphisms (SNPs) is necessary to prescribe effective cancer therapies, perform genetic analyses, and distinguish similar viral strains. Traditionally, SNP sensing uses short oligonucleotide probes that differentially bind the SNP and wildtype targets. However, DNA hybridization-based techniques require precisely tuning the probe's binding affinity to manage the inherent trade-off between specificity and sensitivity. To address this limitation, we generate heteromultivalent DNA-functionalized particles and demonstrate optimized hybridization specificity for targets containing one or two mutations. By investigating the role of oligo lengths, spacer lengths, and binding orientation, we reveal that heteromultivalent hybridization enables fine-tuned specificity for a single SNP and dramatic enhancements in specificity for two non-proximal SNPs empowered by highly cooperative binding. Capitalizing on these abilities, we demonstrate straightforward discrimination between heterozygous cis and trans mutations and between different strains of the SARS-CoV-2 virus. Therefore, heteromultivalent hybridization offers significant improvements over conventional monovalent hybridization-based methods and may significantly impact the fields of diagnostics, genetics, and public health.

Introduction

Specific hybridization between complementary nucleic acids enables many sensing and diagnostic methods.[1-4] For example, PCR assays rely on specific hybridization between primers and templates. However, there is often a fundamental trade-off between maximizing specificity and sensitivity.[5] High binding affinity results in improved sensitivity, allowing the detection of lower concentration oligonucleotides, but also leads to enhanced off-target binding and decreased discrimination between similar targets. Conversely, lowering target affinity can enhance specificity but lowers the limit of detection of an assay. Thus, there is an affinity "sweet spot" that maximizes the ratio between on- and off-target binding.[6] Unfortunately, this optimized affinity is difficult to achieve, often resulting in poor discrimination for targets containing mismatches, such as single nucleotide polymorphisms (SNPs), which are biomedically relevant and challenging to identify.[5, 7-8] Tuning the affinity to maximize specificity can be achieved by changing the probe length. However, the problem with this strategy is that adding or removing a single base pair drastically changes affinity, resulting in low-precision affinity tuning.[6, 9] Adjusting temperature and ionic strength can precisely optimize probe affinity for SNP targets, but this approach fails when detecting multiple SNPs simultaneously in a multiplexed or microarray-type assay.[10] Therefore, a fundamental problem in the field pertains to developing facile strategies to fine tune target affinity and enhance specificity.

To overcome this challenge, we tested the hypothesis that multivalent binding can be used to optimize the specificity of hybridization and hence boost the performance of nucleic acid sensing assays. In many assays, target binding occurs on DNA-functionalized surfaces or particles to allow a more rapid and simple readout.[11-14] These DNA-coated structures, which we refer to as homomultivalent (homoMV) (**Figure 1A, top**), typically hybridize "monovalently", forming a single duplex with each target. There are a few examples of homoMV structures binding targets multivalently, however this approach is only applicable for repetitive targets.[15-16] We recently demonstrated that heteromultivalent (heteroMV) structures presenting multiple distinct oligonucleotide sequences (**Figure 1A, bottom**) can bind multivalently to non-repetitive targets with high avidity.[17] Motivated by this past work, here we investigated if presenting a tuning oligo (T) alongside a SNP-binding oligo (S) can precisely tune target binding affinity and achieve high specificity for a SNP without relying on buffer optimization (**Figure 1B**).

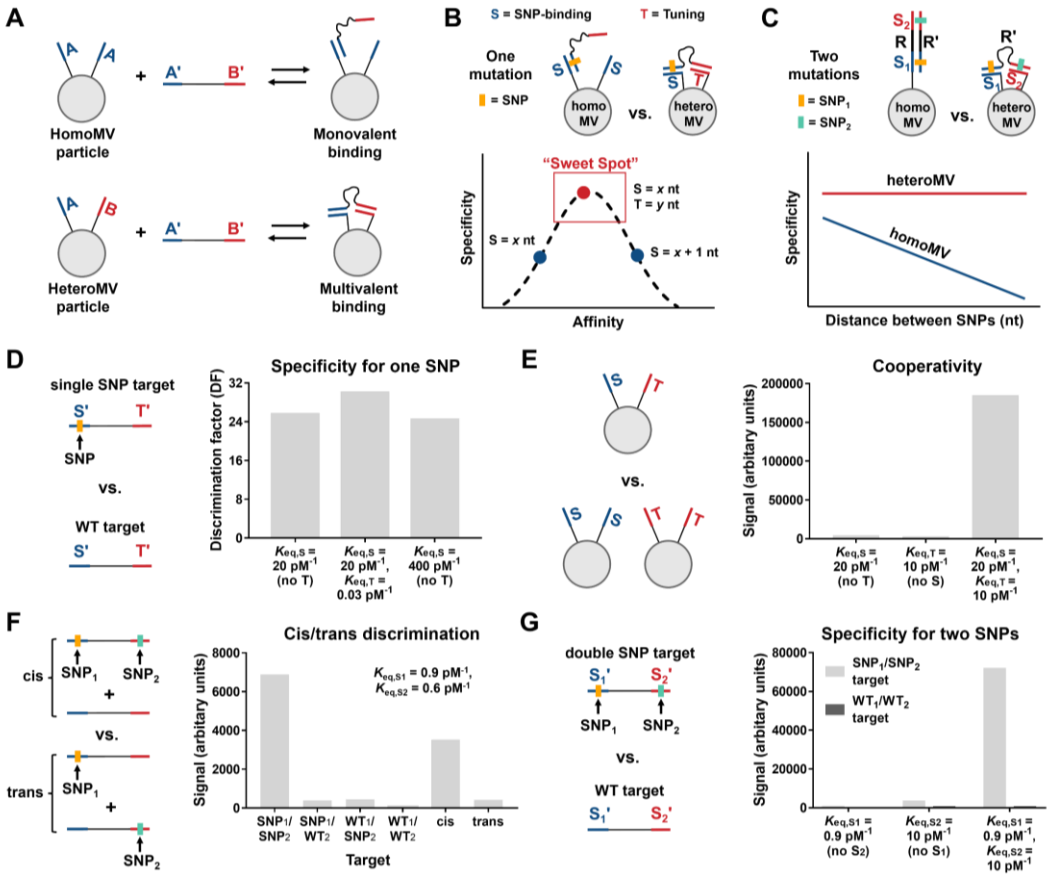

Figure 1. Hypothesized advantages of heteromultivalent hybridization and modeling key applications. (A) General illustration of a homoMV DNA-coated structure containing only one unique oligonucleotide sequence, A, and a heteroMV DNA-coated structure containing two unique oligonucleotide sequences, A and B. (B) Scheme illustrating the difficulty in tuning binding affinity by adding an additional base pair to a homoMV binding interaction and the hypothesized ability of a heteroMV structure to more precisely tune the binding affinity of hybridization to achieve maximum specificity. (C) Scheme illustrating the hypothesized effect of distance between two SNPs on homoMV and heteroMV hybridization specificity. (D-G) Schemes and modeling predictions describing the specificity for one SNP (D), cooperativity (E), cis/trans discrimination (F), and specificity for two SNPs (G) of homoMV and heteroMV particles presenting oligos with the K_{eq} values provided.

Specificity is also important in applications that require detecting multiple mutations in a single target. For example, haplotype phasing analyses involve distinguishing "cis" and "trans" mutations located on the same or different chromosome copy.[18-19] Differentiating viral strains also requires optimizing specificity for unique mutations. However, detecting two mutations on a target is difficult to achieve, as monovalent binding probes bind either both sites and the region in between (R') with low specificity (**Figure 1C**), or bind each mutation separately with no cooperativity. To address this challenge, we engineered heteroMV binding to hybridize cooperatively to two mutations with a non-complementary spacer in between (**Figure 1C**). With heteroMV binding, overall affinity for a desired target is enhanced while maintaining low affinity for single mutant or wildtype targets, similar to "AND" logic gates and proximity assays.[20-22] Moreover, due to the additive effect of each mismatch, we hypothesized that specificity significantly increases when two mutations are targeted through heteroMV binding.

In this work, we studied heteroMV DNA-coated silica microparticles presenting two unique oligo sequences (n=2) of different length that bind to single stranded targets containing a complementary region to each oligo. The two oligos bind single or double mutant targets in several different orientations while the complementary target regions are directly adjacent or separated by a spacer. Through mathematical modeling and a flow cytometry-based assay that allows rapid measurement of target binding to each microparticle, we reveal that heteroMV binding boosts discrimination for a SNP by a factor of up to 10 over monovalent binding when the length of T < S. Moreover, we demonstrate that cooperativity is maximized

when the T and S oligos are tuned such that they bind with similar, yet weak affinities. This high cooperativity persists when binding to two sites of a target separated by an up to 15 nucleotides (nt) long spacer region and can be further improved by modifying the binding orientation of the two oligos. Through precise tuning of both specificity and cooperativity we display the ability to easily distinguish model heterozygous cis and trans mutations. Finally, we apply heteroMV hybridization towards discriminating model SARS-CoV-2 targets corresponding to the Original, Alpha, or Omicron strains and observe ~800-fold binding enhancement for the Omicron target compared to only a ~12-fold enhancement using homoMV particles. Overall, heteroMV binding greatly expands the potential of DNA hybridization-based assays and DNA nanotechnology by offering highly tunable specificity and cooperativity.

Results

Modeling the specificity and cooperativity of heteromultivalent hybridization. To predict the impact of heteroMV binding on hybridization specificity and cooperativity, we focused on a particle modified with 50% S and 50% T oligos. Binding of the target to the particle was modeled as a two-step reversible reaction where S and T bind their complements with binding constants $K_{eq,S}$ and $K_{eq,T}$, respectively. The particle-target complex can form three distinct binding states where only S binds, only T binds, or where both segments bind (**Figure S2**). The equilibrium constant for the target bound to both segments can be described as:

$$K_{eq} = K_{eq,S} * K_{eq,T} * c_{eff} \quad (1)$$

where c_{eff} is the effective concentration of the unbound second oligo within the volume accessible to the target after binding the first oligo. Thus, the total affinity of all three states for the particle binding a complementary SNP-containing target is:

$$K_{eq,S+T,SNP} = K_{eq,S} + K_{eq,T} + K_{eq,S} * K_{eq,T} * c_{eff} \quad (2)$$

To incorporate specificity into the model, we also derived a binding constant for a wildtype target (WT) containing a mismatch in S' (**Figure 1D**). To account for the decreased affinity of the mismatched S oligo-WT target duplex, a mismatch factor (MM) is multiplied to each $K_{eq,S}$ term in equation 2. Therefore, the total binding affinity for the particle binding the WT target is:

$$K_{eq,S+T,WT} = MM * K_{eq,S} + K_{eq,T} + MM * K_{eq,S} * K_{eq,T} * c_{eff} \quad (3)$$

We next derived an equation to calculate the equilibrium binding occupancy, Θ, of the particle-functionalized oligos and converted Θ to an arbitrary assay signal, I, using inputted maximum and background assay signals (**see Methods**). By calculating I when the particles bound the SNP target or the WT target, the discrimination factor (DF) was calculated using the equation:

$$DF = I_{SNP} / I_{WT} \quad (4)$$

Moreover, by calculating I when a particle with only the S oligo, only the T oligo, or both oligos bound the SNP target (**Figure 1E**), the cooperativity factor (CF) was calculated using the equation:

$$CF = 2 * I_{S+T} / (I_S + I_T) \quad (5)$$

To predict the impact of $K_{eq,S}$ and $K_{eq,T}$ on DF and CF, we ran numerical analyses using a series of affinities for each oligo with values spanning many orders of magnitude. The incremental change in affinity between each binding constant roughly approximated the impact of adding one additional base pair to a DNA duplex. Mock values of I, DF, and CF were then generated for each combination of $K_{eq,S}$ and $K_{eq,T}$ (**Figure S2**). As described previously for monovalent hybridization,[6] the relationship between DF and K_{eq} follows a Gaussian distribution, where a specific K_{eq} value ($K_{eq,optimal}$) maximizes DF (DF_{max}) and any K_{eq} value less than or greater than $K_{eq,optimal}$ results in a diminished DF (**Figure S1**). For example, our modeling predicts that for an S only particle, increasing $K_{eq,S}$ from 20 to 400 pM^{-1} (representing the addition of one base pair to the duplex) overshoots $K_{eq,optimal}$ and thus DF_{max} is not achieved. However, adding a T oligo with $K_{eq,T}$ = 0.03 pM^{-1} instead precisely increases the total affinity from 20 to 40 pM^{-1} and yields a DF greater

than that of any of the n=1 particles in the series (**Figure 1D**). Note that the model predicts that the T oligo will not enhance DF_{max} and also that if $K_{eq,T}$ is too large (regardless of $K_{eq,S}$), then DF_{max} will decrease (**Figure S2**).The second major prediction from this simple model is that CF will be greatest when $K_{eq,S} \approx K_{eq,T}$. Specifically, when $K_{eq,S}$ = 20 pM^{-1} and $K_{eq,T}$ = 10 pM^{-1} the model predicts that the n=2 particle will bind ~50x more targets than the average of the two corresponding n=1 particles (**Figure 1E**).

We next sought to predict whether heteroMV DNA-coated structures can be used to determine if two mutations are located on the same or different chromosome copies. Of the 10 unique combinations of two mutations on two chromosome copies (**see Methods**), heterozygous cis and trans mutations are the most difficult to distinguish (**Figure 1F**).[23-24] To predict the ability to differentiate two cis or trans mutations, the model was modified so that both oligos (S_1 and S_2) are complementary to a SNP by applying a MM factor to $K_{eq,S1}$ and $K_{eq,S2}$ when binding a target lacking the corresponding SNPs. This modification then yields equations for total affinity to the SNP_1/SNP_2, SNP_1/WT_2, WT_1/SNP_2, and WT_1/WT_2 targets (**see Methods**). Equal mixtures of SNP_1/SNP_2 and WT_1/WT_2 targets or SNP_1/WT_2 and WT_1/SNP_2 targets were used to represent heterozygous cis or trans mutations, respectively. $DF_{cis/trans}$ values were then calculated using the equation:

$$DF_{cis/trans} = I_{cis} / I_{trans} \qquad (6)$$

Using the same individual oligo binding affinities as used in **Fig. 1D and 1E**, the $DF_{cis/trans}$ values were generated for each combination of $K_{eq,S1}$ and $K_{eq,S2}$ (**Figure S3**). These modeling calculations predicted that two oligos with roughly equal binding affinities, slightly weaker than those predicted to give the best CF, will result in the highest $DF_{cis/trans}$ (**Figure 1F**). Alternatively, to maximize $DF_{SNP1+SNP2}$ ($I_{SNP1/SNP2}$ / $I_{WT1/WT2}$) to ~300, our calculations suggest that a total affinity between the affinities that yielded the best CF and $DF_{cis/trans}$ values is optimal (**Figure 1G and S3**). Note that $DF_{SNP1+SNP2}$ is significantly enhanced due to both binding interactions being impacted by the presence of SNPs. Overall, the mathematical model predicts that a T oligo with lower affinity than the S oligo will give the highest specificity for a single mismatch, a T oligo with similar affinity to the S oligo will maximize cooperativity, and two S oligos with equal but weak affinity will offer the highest cis/trans discrimination or specificity for targets containing two mutations.

Measuring the specificity and cooperativity of heteromultivalent hybridization. To test the modeling predictions, we designed five S oligos (7-11 nt long, 7S-11S) and seven T oligos (4-10 nt long, 4T-10T) complementary to a 25 nt region of the KRAS genetic sequence that contains the G12C mutation (**Figure 2A and Figure S4**). We focused on this target because KRAS is an important oncogene and a driver of lung, pancreatic, and colorectal cancers when mutated.[25] The G12C mutant target was perfectly complementary to the S and T oligos, whereas the WT target lacking the mutation binds the S oligo with a single base mismatch and the T oligo with no mismatches. Both targets were modified at their 3' termini with an Atto647N fluorophore (**Figure S5 and Figure S6**). Each of the S and T oligos contained a T10 polynucleotide linker and a 5' thiol group to enable conjugation to silica beads (**Figure S7**). Beads were modified with each possible combination of the S and T oligos, generating a library of 48 unique DNA-coated silica beads. The density of the oligos on the beads were measured by first dissolving the beads in 0.1 M KOH as demonstrated previously[26] and then using Oligreen reagent to quantify the amount of DNA in solution. These measurements revealed that there were ~4.1 x 10^4 oligos/μm^2 and an average oligo spacing of ~5 nm, allowing S and T oligos to bind multivalently to the same target (**Figure S8**). Fluorescence microscopy was also used to image targets hybridized to the beads and confirmed homogeneous binding across the bead surface (**Figure S9**).

We next designed a flow cytometry-based assay to measure relative binding of targets to each of the 48 beads. In this assay, the DNA-coated beads were incubated with 1 nM of target in 1x SSC and 0.1% Tween20 buffer, after which unbound targets were removed through centrifugation and the fluorescence intensity of each individual particle was measured using a flow cytometer (**Figure 2B and Figure S10**). As expected, median fluorescence intensities (MFIs) generally increased when the S and/or the T oligo increased in length, confirming that increasing binding affinity results in higher surface occupancy (Θ) (**Figure 2C, 2D, and S11**). To quantify specificity, DF values were calculated for each bead mixture by dividing the G12C and WT MFIs (**Figure 2E**). Consistent with the modeling predictions, the beads presenting the 9S oligo alongside the 5T, 6T, or 7T oligo had the highest DFs. Specifically, the 5T-9S beads yielded ~37% higher specificity compared to the 9S beads (**Figure 2I**), which had the greatest DF of the homoMV beads tested. Importantly, this enhancement was enabled by precise fine-tuning of K_{eq} as the 5T-

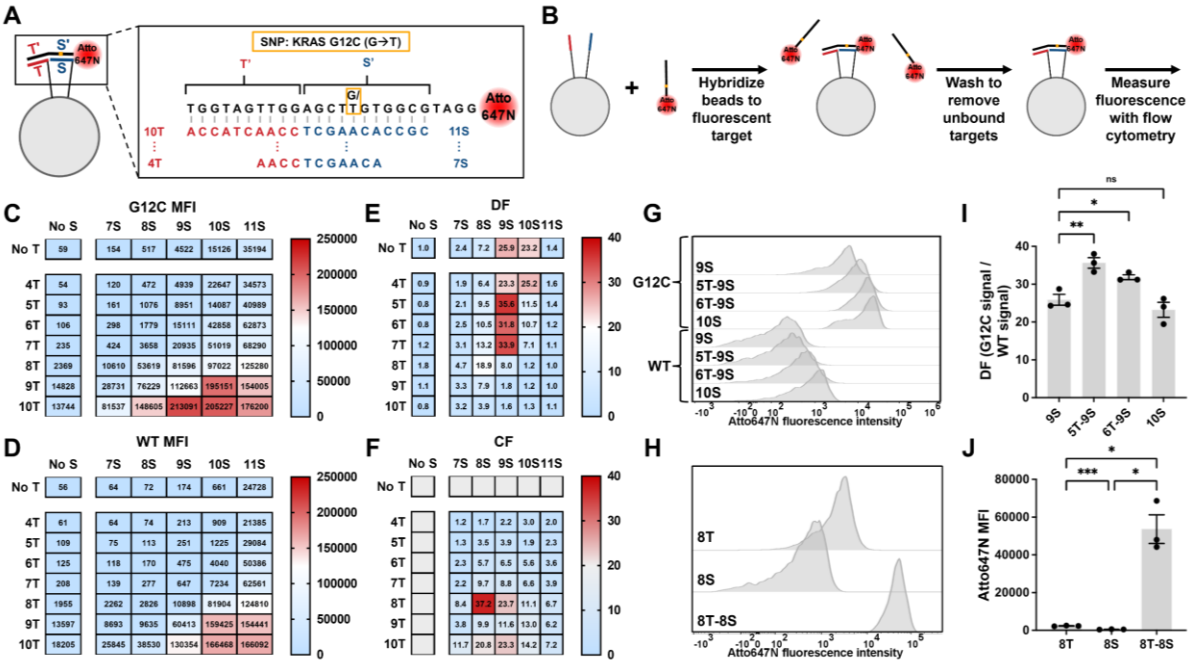

Figure 2. Measuring the specificity and cooperativity of heteromultivalent hybridization. (A) Design of the oligonucleotides included in the screen to maximize discrimination factor and cooperativity factor. Yellow boxes describe the SNP and its position in the target sequence. (B) Scheme describing the flow cytometry-based assay used to quantify target binding to 5 µm DNA-coated silica particles. (C and D) Heatmaps showing the median fluorescence intensity of each bead included in the screen when incubated with the G12C target (C) and the WT target (D). (E and F) Heatmaps showing the discrimination factor (E) and cooperativity factor (F) of each bead included in the screen. The cooperativity factor is shown for beads incubated with the G12C target. (G) Representative histograms for 9S, 5T-9S, 6T-9S, and 10S beads binding the G12C and WT targets. (H) Representative histograms for 8T, 8S, and 8T-8S beads binding the G12C target. (I) Measured discrimination factors for 9S, 5T-9S, 6T-9S, and 10S beads. (J) Measured median fluorescence intensity values for 8T, 8S, and 8T-8S beads binding the G12C target. Error bars represent standard error of the mean. Values were compared using paired one-way ANOVA with multiple comparisons follow-up tests ($^{ns}P > 0.05$, *P < 0.05, **P < 0.01, ***P < 0.001).

9S and 6T-9S beads yielded MFIs between that of the 9S and 10S beads (**Figure 2G**). In further agreement with the modeling, the screen showed that the 8T-8S beads bound most cooperatively to the G12C target, with almost 40x greater target binding than the average of the 8T and 8S *n*=1 beads (**Figure 2F, 2H, and 2J**).

Determining the impact of spacer length on heteromultivalent hybridization specificity and cooperativity. Next, to assess the ability of heteroMV beads to bind with high cooperativity to two non-adjacent regions of a target, several spacer-containing targets were designed and tested. Previously, the impact of long, flexible spacers/linkers on multivalent binding avidity has been a controversial topic. Some studies reported that flexibility leads to poor cooperativity due to loss of conformational entropy upon binding,[27] while others noted minimal impacts of spacer length on avidity and cooperativity.[15, 28] Hence these experiments were designed to test whether hybridization cooperativity and specificity are maintained when the spacer length increases. We therefore introduced a tri-ethylene glycol (short) or a hexa-ethylene glycol (long) modification between the T' and S' binding regions (internal) or, as a negative control, at the 5' terminus of the targets (terminal) (**Figure 3A**). Thus, a total of 10 targets were tested with the 8T-8S beads using the flow cytometry-based assay.

The results showed that as internal spacer length increased, more G12C targets bound the beads (**Figure 3B**). Inserting a short spacer also enhanced binding to the WT target though the long spacer did not lead to a further increase in binding (**Figure 3C and Figure S12**). As expected, the terminal spacers did not impact binding to the G12C or WT targets, confirming that the poly-ethylene glycol (PEG) polymer

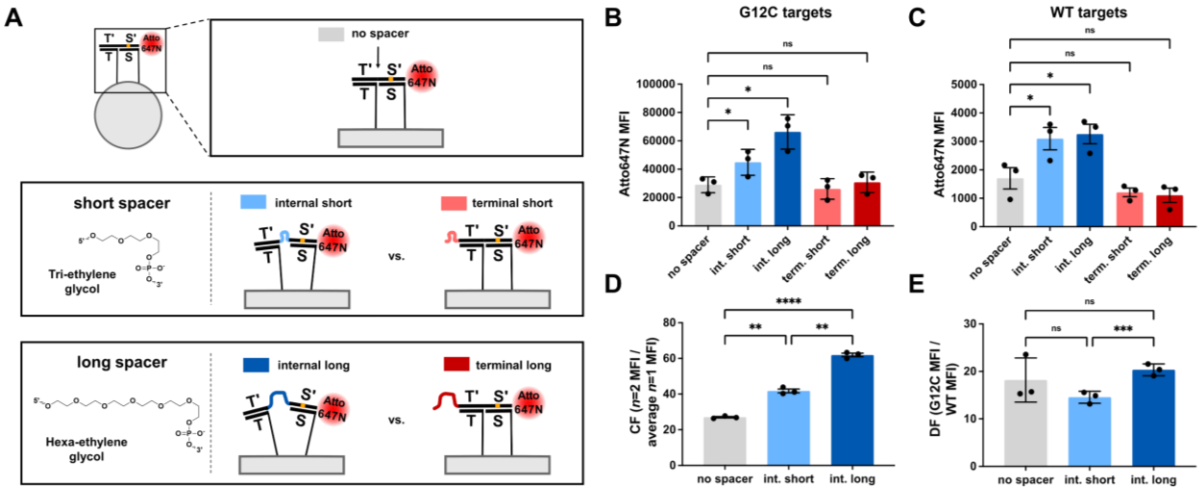

Figure 3. Determining the impact of spacer length on heteromultivalent hybridization specificity and cooperativity. (A) Scheme describing the design of the no spacer target, the internal and terminal short spacer targets, and the internal and terminal long spacer targets including the chemical structures of the PEG spacer molecules. (B and C) Measured median fluorescence intensity values for 8T-8S beads binding the G12C (B) and the WT (C) no spacer, internal short spacer, internal long spacer, terminal short spacer, and terminal long spacer targets. (D and E) Measured cooperativity factors (D) and discrimination factors (E) for the 8T-8S beads binding the G12C no spacer, internal short spacer, or the internal long spacer targets. Error bars represent standard error of the mean. Values were compared using paired one-way ANOVA with multiple comparisons follow-up tests ($^{ns}P > 0.05$, *P < 0.05, **P < 0.01, ***P < 0.001, ****P < 0.0001).

does not chemically influence target binding. The CF of the 8T-8S beads for the G12C targets with different spacer lengths was also calculated by dividing the 8T-8S beads' MFI by the average of the 8T and 8S beads' MFIs when binding the no spacer target. These calculations revealed significant increases in cooperativity as a function of increasing spacer length (**Figure 3D**). The impact of spacer length on specificity was also assessed by calculating the DF of the 8T-8S beads for each target. Interestingly, the internal spacers did not lead to a strong effect on specificity, though there was a significant difference in DF between the short and long spacer targets (**Figure 3E**). Surprisingly, 8T and 8S only beads also showed increased binding to the internal spacer-containing targets, potentially due to weak binding between S' and T as well as T' and S (**Figure S12**). Overall, the investigations into the effect of target spacer length revealed that heteroMV hybridization allows binding to two spacer-separated regions of a target with increased cooperativity and no loss in specificity compared to a target with no spacer. These results will provide guidance in potential designs of proximity or "AND" logic gate style-assays as well as in diagnostic assays when it is desirable for the tuning oligo to bind a domain (T') that is not proximal to the SNP site.

Determining the impact of binding orientation on heteromultivalent hybridization specificity and cooperativity. Due to the antiparallel nature of DNA hybridization, the choice of terminus (5' or 3') for the anchoring group of the S and T oligos impacts the direction that the oligo binds the target. Therefore, based on the terminus used for each anchor, the two oligos can bind the target in a head-to-tail, head-to-head, or tail-to-tail orientation (**Figure 4A**). In this case, head corresponds to the end of the oligo not attached to the particle and tail corresponds to the linker connecting the oligo to the particle. To understand how binding orientation can potentially impact the properties of the binding interaction, 8T-8S beads that bind in the three different orientations were compared using the flow cytometry-based binding assay. Moreover, to investigate how each orientation is influenced by spacer length, the no spacer, short spacer, and long spacer targets were tested with each binding orientation.

When binding the G12C no spacer target, significant differences were observed between the three binding orientations (**Figure 4B and 4C**). Specifically, the head-to-head binding orientation yielded the highest binding, while the tail-to-tail orientation resulted in a >3-fold reduction in binding compared to the head-to-tail orientation. However, when binding the short or long spacer G12C targets, the tail-to-tail orientation yielded similar binding to the head-to-tail orientation, while the head-to-head orientation still offered slight, non-significant improvements in total binding. Relatedly, the head-to-head orientation beads

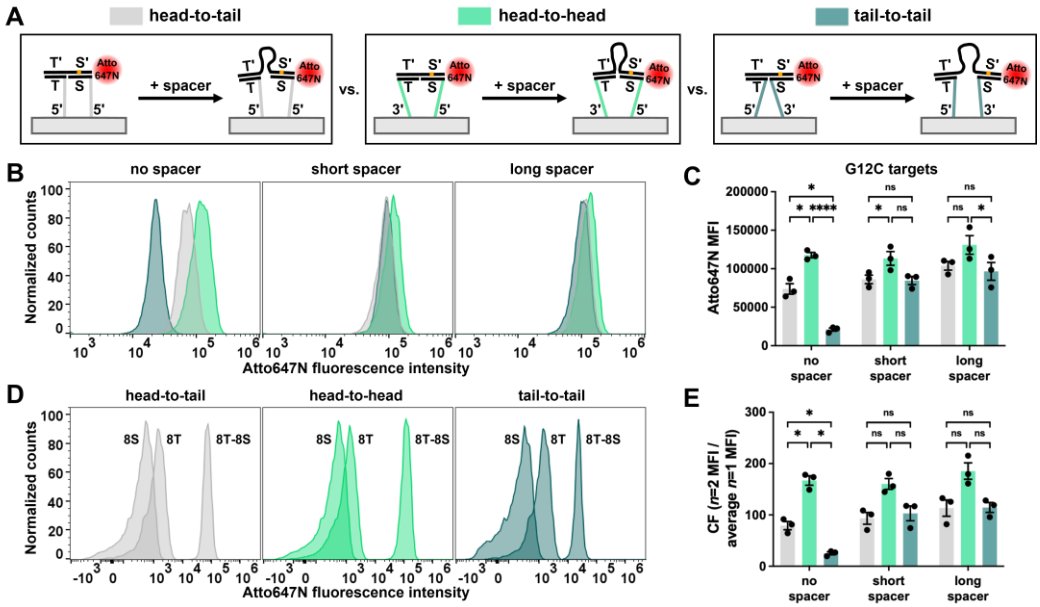

Figure 4. Determining the impact of binding orientation on heteromultivalent hybridization specificity and cooperativity. (A) Scheme describing *n*=2 beads with head-to-tail, head-to-head, or tail-to-tail orientation binding to targets with or without a spacer region. (B and C) Representative histograms (B) and measured median fluorescence intensity values (C) for 8T-8S beads with each orientation binding the G12C no spacer, short spacer, and long spacer targets. (D) Representative histograms for 8T, 8S, and 8T-8S beads with each orientation binding the G12C no spacer target. (E) Measured cooperativity factors for 8T-8S beads with each orientation binding the G12C no spacer, short spacer, and long spacer targets. Error bars represent standard error of the mean. Values were compared using paired one-way ANOVA with multiple comparisons follow-up tests ($^{ns}P > 0.05$, *P < 0.05, ****P < 0.0001).

had a significant >2-fold increase in CF relative to the head-to-tail orientation beads and a >6-fold increase relative to the tail-to-tail orientation beads when binding the no spacer G12C target (**Figure 4D and 4E**). The greater average CF for the head-to-head orientation was maintained for the spacer-containing targets, though the enhancement was not significant. The results for the WT target echoed those of the G12C target, and as expected, the oligo's anchoring terminus did not have a significant effect on *n*=1 beads binding the G12C no spacer target (**Figure S13**). Overall, these results validate the importance of binding orientation in tuning binding affinity and cooperativity.

Together, these results can be explained by considering the effects of both the spacing between segments on the bead surface and the base stacking interactions at the interface of the T-T' and S-S' duplexes. Based on the distance between the T and S oligos on the surface, different binding orientations can minimize energetic strain during binding depending on linker length and duplex length. For example, if T and S are far apart, then binding the no spacer target in the tail-to-tail orientation might result in significant strain on the T10 linkers. Moreover, prior studies showed that base stacking at a nick site can result in strong enthalpic contributions to overall binding stability.[29-32] This is consistent with the head-to-head orientation yielding the most avid binding as it binds with only a nick between the two duplexes. In contrast, in the other orientations, the T10 linkers likely interfere with this base-stacking interaction and hence reduce binding affinity and cooperativity.

Detecting the cis/trans relationship of two mutations using heteromultivalent hybridization. We next tested the modeling prediction that heteroMV binding can be used to distinguish heterozygous cis and trans mutations (**Figure 1F and 5A**). This challenging task is significant in medical diagnostics as the presence of two mutations on the same gene copy can alter protein function, while one mutation on each gene copy can yield cells with no functional gene copies.[18, 23-24] Moreover, cis/trans discrimination is significant in genetic counseling in order to track the inheritance of mutations.[18] As a proof-of-concept, 8 and 9 nt S_1 and S_2 oligos were designed to hybridize in the head-to-tail or head-to-head orientation to a complementary 31 nt target corresponding to a region of the KRAS gene which contains the G12C mutation (SNP_1) in the S_1'

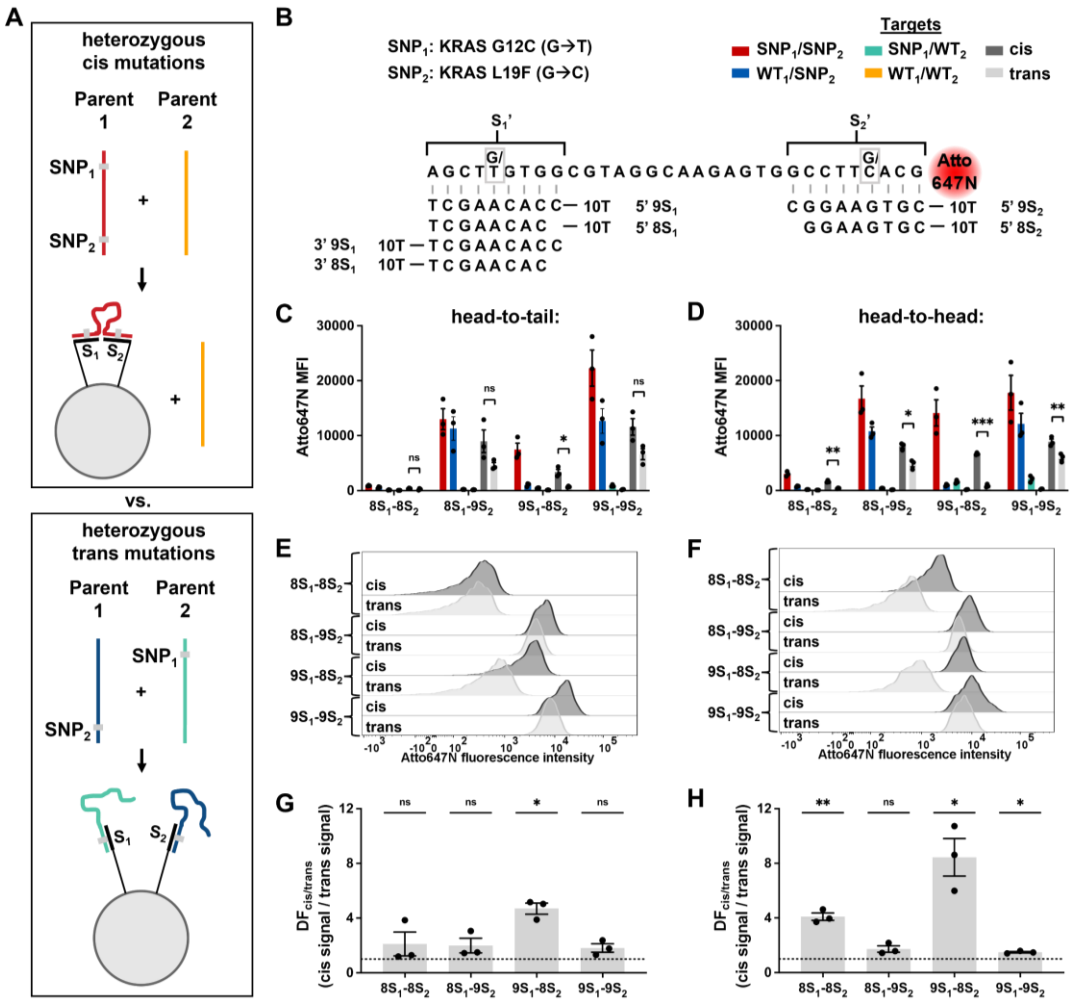

Figure 5. Detecting the cis/trans relationship of two mutations using heteromultivalent hybridization. (A) Scheme illustrating the use of head-to-head orientation heteromultivalent DNA-coated beads to distinguish the heterozygous cis mutations mixture (red and yellow targets) from the heterozygous trans mutations mixture (blue and green targets). Ideally, the double mutant target (red) will bind the beads multivalently with high affinity, the single mutant targets (blue and green) bind monovalently with low affinity, and the no mutant target (yellow) shows negligible binding. (B) Scheme describing the sequence of the binding oligos, identity of the two SNPs, and the two binding orientations tested. (C and D) Measured median fluorescence intensity values for each bead with head-to-tail orientation (C) or head-to-head orientation (D) binding each of the targets or target combinations in the legend. Values were compared using paired student t tests ($^{ns}P > 0.05$, *P < 0.05, **P < 0.01, ***P < 0.001). (E and F) Representative histograms for each bead with head-to-tail orientation (E) or head-to-head orientation (F) binding the cis or trans target combinations. (G and H) Measured cis/trans discrimination factors for each bead with head-to-tail orientation (G) or head-to-head orientation (H). Values were compared to baseline value of 1 (dotted black line) using one-sample t tests ($^{ns}P > 0.05$, *P < 0.05, **P < 0.01). Error bars represent standard error of the mean.

region and the L19F mutation (SNP_2) in the S_2' region (**Figure 5B and Figure S4**). Between the S_1' and S_2' regions there are 13-15 non-complementary nt (**Figure S14**). L19F is a non-canonical mutation that has been found to cause increased tumor proliferation and transforming potential over WT KRAS.[33] We chose to use this mutation in our assay due to its proximity to the G12C mutation (23 nt away), though we anticipate binding two mutations that are further apart will still be effective.

Using each combination of the binding oligos, 8 heteroMV beads were synthesized and flow cytometry was used to measure their binding to 1 nM of the four targets, as well as to a 0.5 nM of SNP_1/SNP_2 + 0.5 nM of WT_1/WT_2 target mixture (cis) or a 0.5 nM of SNP_1/WT_2 + 0.5 nM of WT_1/SNP_2 target mixture (trans) (**Figure 5C, 5D, and S14**). As expected, all the bead combinations bound the SNP_1/SNP_2 target with the greatest affinity and the WT_1/WT_2 target with the weakest affinity. Moreover, the $9S_1$-$8S_2$ beads

with either binding orientation had weak and approximately equal binding to both single mutant targets while showing strong binding to the SNP_1/SNP_2 target, yielding DF values ~10 for both mutations. Due to this specificity for both mutations and strong binding cooperativity, both the head-to-tail and head-to-head $9S_1$-$8S_2$ beads bound the cis target combination significantly more than the trans with $DF_{cis/trans}$ values of 4.7 and 8.4, respectively (**Figure 5E-H**). Interestingly, both beads containing the $8S_2$ oligo had higher $DF_{cis/trans}$ values when binding in the head-to-head orientation. Alternatively, beads containing the $9S_2$ oligo bound the SNP_1/SNP_2 and WT_1/SNP_2 targets similarly, resulting in poor specificity for SNP_1, and had similar $DF_{cis/trans}$ values in both orientations. This suggests that the $9S_2$ oligo's affinity for the target is too high resulting in low cooperativity binding that is not impacted by a mismatch in the S_1' region. These results offer further evidence that the head-to-head orientation can yield higher binding, particularly when the two immobilized oligos are binding cooperatively. Overall, this screen reveals that heteroMV hybridization enables strong discrimination between cis and trans heterozygous mutations and demonstrates the importance of precisely tuned binding specificity and cooperativity. This result is important as it establishes a hybridization-based approach to distinguish cis/trans mutations without using enzymes or magnetic separation techniques.[24, 34-36]

Distinguishing different strains of SARS-CoV-2 using heteromultivalent hybridization. We next tested our hypothesis that heteroMV hybridization could lead to dramatic enhancements in specificity for targets containing two mutations (**Figure 1G**). We thus designed three model targets corresponding to a 29 nt region of the SARS-CoV-2 spike protein gene that contains three mutations (Q498R, N501Y, and Y505H) in the Omicron strain, one mutation in the Alpha strain (N501Y), and no mutations in the Original strain (**Figure 6A**). To hybridize specifically to the Omicron strain, 8 and 9 nt S_1 and S_2 oligos, complementary to the Q498R site and the Y505H site respectively, were designed so that neither overlap with the N501Y mutation shared by the Alpha strain (**Figure 6B**). Using these oligos, four *n*=2 beads were synthesized that bound the target in the head-to-head orientation with an 11-13 nt spacer region (**Figure S15**). As a negative control, *n*=1 beads functionalized with a 29 nt oligo that is perfectly complementary to the Omicron target were also tested (**Figure 6B**). Flow cytometry results showed that each of the *n*=2 beads tested bound to the Omicron target with similarly high affinity and showed minimal binding to the Alpha and Original targets (**Figure S15**). Meanwhile, compared to the *n*=2 beads, the *n*=1 beads yielded an approximately equal MFI when binding the Omicron target but bound to significantly more Alpha and Original targets (**Figure 6C and 6D**). Importantly, the *n*=2 beads offered dramatically enhanced specificity for the Omicron strain, with the $8S_1$-$9S_2$ combination bead giving a $DF_{SNP1 + SNP2}$ value of ~800 compared to either of the other targets (**Figure 6E**). The *n*=1 bead had much lower specificity for the Omicron target with $DF_{SNP1 + SNP2}$ values of ~12.

As the *n*=1 bead has more total complementarity with the targets, it was surprising that the *n*=1 and *n*=2 beads yielded approximately equal Omicron target binding. Potential explanations include increased secondary structure, reduced k_{on} rates, and reduced DNA density for the *n*=1 bead as has been previously observed for materials functionalized with longer oligos,[37-39] though these hypotheses were not tested herein. This highlights a general advantage for heteroMV hybridization where each oligo can be shorter in length and therefore less likely to be impacted by these issues. Moreover, the stark differences in specificity between the *n*=1 and *n*=2 beads would likely become even greater as the inter-SNP distance increases (**Figure 1C**). In this case, the length of the oligo on the *n*=1 bead would have to become longer to bind to both SNPs, while the oligos on the *n*=2 beads would not need to be altered, and instead potentially exhibit stronger and more cooperative binding as shown in **Figure 4**. Interestingly, the $DF_{SNP1 + SNP2}$ values obtained were even higher than predicted (**Figure 1G**), possibly a result of increased secondary structure for the Original and Alpha targets relative to the Omicron target (**Figure S4**). This demonstration of rapid and effective identification of the strain of model viral targets using heteroMV hybridization has the potential to significantly impact the fields of diagnostics, medicine, and public health.

Discussion

In this report, we show that densely coating a microparticle with two distinct oligonucleotide sequences yields customizable multivalent binding with highly tunable affinity. This result led to several important capabilities. By first optimizing each oligo's length, we show that heteroMV binding can control binding strength more precisely than monovalent binding, enabling near-maximum discrimination of SNPs. Thus, heteroMV hybridization offers an approach to optimizing the performance of hybridization-based

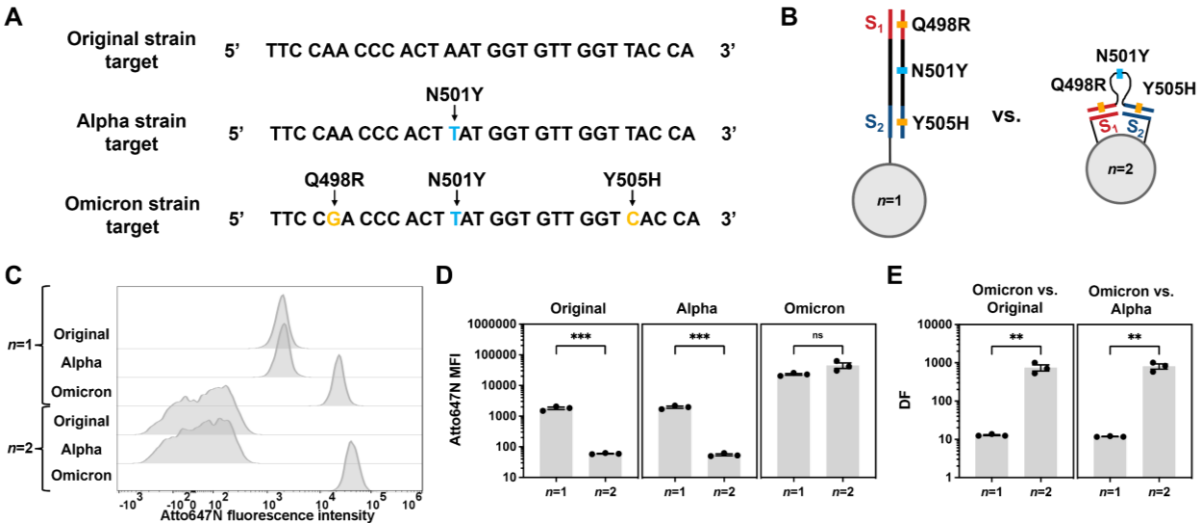

Figure 6. Distinguishing different strains of SARS-CoV-2 using heteromultivalent hybridization. (A) Sequences of targets based on the Original, Alpha, and Omicron strains of SARS-CoV-2 spike protein, with the mutations in each target indicated with arrows. (B) Scheme describing the binding of an *n*=1 bead functionalized with an oligo that is fully complementary to the Omicron target and the binding of an *n*=2 bead functionalized with S_1 and S_2 oligos that are complementary to the regions of the target containing the Q498R and Y505H mutations but not the N501Y mutation. (C and D) Representative histograms (C) and measured median fluorescence intensity values (D) for the *n*=1 and $8S_1$-$9S_2$ *n*=2 beads binding each target. (E) Measured discrimination factors for the *n*=1 and $8S_1$-$9S_2$ *n*=2 beads binding the Omicron target vs. the Original target or the Omicron target vs. the Alpha target. Values were compared using unpaired student t tests ($^{ns}P > 0.05$, $^{**}P < 0.01$, $^{***}P < 0.001$). Error bars represent standard error of the mean.

mutation detection tools while maintaining compatibility with multiplex assays. While different mutations and assay conditions will still require optimization of the oligo lengths to tune specificity, the results herein will accelerate future screening processes. Moreover, heteroMV binding can be combined with other approaches that are commonly used to enhance binding specificity, such as molecular beacon, toehold-mediated hybridization, and competition/sink probes.[3, 5-8]

In addition to adjusting the oligo length, customizing the spacer length and binding orientation allowed demonstration of highly cooperative binding to two unique regions of a target. Both parameters are thus critical for applications that necessitate selective hybridization only when two receptors are present.[21] Enhanced cooperativity was also observed as spacer length increased, potentially due to improved ability for a target to reach two adjacent surface oligos. Additionally, as the spacer length increases, the target can span longer distances on the particle surface allowing access to more copies of each binding oligo. These added binding partners, though spread through a larger volume, can result in a higher local concentration of surface-bound oligos.[40] This feature is unique to heteroMV structures that are densely functionalized, as opposed to a structure that presents a single copy of each oligo and thus cannot access additional binding sites despite a longer spacer. Cooperative binding was demonstrated with up to 15 nt spacers, though further studies with longer spacers would deepen the investigation. Furthermore, when binding the target lacking a spacer, a 6-fold increase in cooperativity was observed when head-to-head orientation was used instead of tail-to-tail. However, for heteroMV binding where *n*>2, it is not possible to exclusively use the highly cooperative head-to-head orientation. Instead, each adjacent oligo pair must alternate between binding in the head-to-head and tail-to-tail orientation or each oligo can be anchored through the same terminus, as previously demonstrated.[17]

Through the combined benefits of highly tunable affinity and strong cooperativity despite a spacer region in the target, heteroMV binding also resulted in the ability to distinguish heterozygous cis and trans mutations. Through optimization, ~8-fold higher binding was observed when heteroMV particles were incubated with a mixture of double mutant and non-mutant targets rather than two single mutant targets. Distinguishing between these target mixtures is often achieved through costly and lengthy methods involving complex next-gen sequencing assays, droplet PCR, or single-molecule dilution.[18-19] Alternatively,

in monovalent hybridization-based assays either one long probe is used to bind both mutations or a distinct probe binds each mutation. In the first case, specificity and cooperativity diminish due to excessively strong binding, while in the second case each probe binds identically to cis and trans target mixtures.[24] For this reason, hybridization-based assays typically rely on a second discriminatory step involving enzymes or separation techniques.[24, 34-35] Finally, heteroMV hybridization enabled ~800-fold higher binding when targeting two SNPs unique to the Omicron strain of the SARS-CoV-2 genome over that of the original strain. Note that whole-genome sequencing is typically performed for strain identification. Thus, the ability to rapidly determine the strain of the viral sample offers facile monitoring of viral evolution.

The heteroMV hybridization approach presented herein is compatible with many materials used to present oligos in close-proximity, including 1, 2, or 3-dimensional structures.[15-16] Also, functionalizing the material heteromultivalently is straightforward as oligo spatial patterning does not significantly impact binding affinity when *n* is low.[17] Moreover, precisely controlling the inter-oligo distance on the surface is not necessary when target binding regions are further apart as such targets can span longer distances without diminished cooperativity. The cooperativity arising from heteroMV binding does however depend on the oligos being pre-linked to a scaffold. Alternatively, "binary" probes have been described, which rely on monovalent binding of two unlinked oligo probes and a separate complex formation step to generate a signal.[10, 41] Additionally, DNA origami nanoswitches have been engineered to switch to a loop conformation upon heteroMV binding to a target to facilitate detection with gel electrophoresis.[22, 42] In this work, fluorophore-labeled targets were used to enable a rapid flow cytometry readout but for diagnostic applications requiring unlabeled target sensing, an altered readout method is necessary. In many nucleic acid detection methods, tunable binding affinity that allows highly specific and cooperative binding is essential, and therefore, heteroMV DNA hybridization is a promising method for further advancing biomedical sensing and diagnostics.

References

1. Gunderson, K. L.; Steemers, F. J.; Lee, G.; Mendoza, L. G.; Chee, M. S., A genome-wide scalable SNP genotyping assay using microarray technology. *Nat Genet* **2005,** *37* (5), 549-54.
2. Koltai, H.; Weingarten-Baror, C., Specificity of DNA microarray hybridization: characterization, effectors and approaches for data correction. *Nucleic Acids Res* **2008,** *36* (7), 2395-405.
3. Tyagi, S.; Bratu, D. P.; Kramer, F. R., Multicolor molecular beacons for allele discrimination. *Nat Biotechnol* **1998,** *16* (1), 49-53.
4. Tulpan, D.; Andronescu, M.; Chang, S. B.; Shortreed, M. R.; Condon, A.; Hoos, H. H.; Smith, L. M., Thermodynamically based DNA strand design. *Nucleic Acids Res* **2005,** *33* (15), 4951-64.
5. Chen, X.; Liu, N.; Liu, L.; Chen, W.; Chen, N.; Lin, M.; Xu, J.; Zhou, X.; Wang, H.; Zhao, M.; Xiao, X., Thermodynamics and kinetics guided probe design for uniformly sensitive and specific DNA hybridization without optimization. *Nat Commun* **2019,** *10* (1), 4675.
6. Zhang, D. Y.; Chen, S. X.; Yin, P., Optimizing the specificity of nucleic acid hybridization. *Nat Chem* **2012,** *4* (3), 208-14.
7. Wang, J. S.; Zhang, D. Y., Simulation-guided DNA probe design for consistently ultraspecific hybridization. *Nat Chem* **2015,** *7* (7), 545-53.
8. Tyagi, S.; Kramer, F. R., Molecular beacons: probes that fluoresce upon hybridization. *Nat Biotechnol* **1996,** *14* (3), 303-8.
9. Suzuki, S.; Ono, N.; Furusawa, C.; Kashiwagi, A.; Yomo, T., Experimental optimization of probe length to increase the sequence specificity of high-density oligonucleotide microarrays. *BMC Genomics* **2007,** *8*, 373.
10. Kolpashchikov, D. M., Binary probes for nucleic acid analysis. *Chem Rev* **2010,** *110* (8), 4709-23.
11. Taton, T. A.; Mirkin, C. A.; Letsinger, R. L., Scanometric DNA array detection with nanoparticle probes. *Science* **2000,** *289* (5485), 1757-60.
12. Alhasan, A. H.; Kim, D. Y.; Daniel, W. L.; Watson, E.; Meeks, J. J.; Thaxton, C. S.; Mirkin, C. A., Scanometric microRNA array profiling of prostate cancer markers using spherical nucleic acid-gold nanoparticle conjugates. *Anal Chem* **2012,** *84* (9), 4153-60.
13. Diehl, F.; Li, M.; Dressman, D.; He, Y.; Shen, D.; Szabo, S.; Diaz, L. A., Jr.; Goodman, S. N.; David, K. A.; Juhl, H.; Kinzler, K. W.; Vogelstein, B., Detection and quantification of mutations in the plasma of patients with colorectal tumors. *Proc Natl Acad Sci U S A* **2005,** *102* (45), 16368-73.

14. Schena, M.; Shalon, D.; Davis, R. W.; Brown, P. O., Quantitative monitoring of gene expression patterns with a complementary DNA microarray. *Science* **1995,** *270* (5235), 467-70.
15. Curk, T.; Brackley, C. A.; Farrell, J. D.; Xing, Z.; Joshi, D.; Direito, S.; Bren, U.; Angioletti-Uberti, S.; Dobnikar, J.; Eiser, E.; Frenkel, D.; Allen, R. J., Computational design of probes to detect bacterial genomes by multivalent binding. *Proc Natl Acad Sci U S A* **2020,** *117* (16), 8719-8726.
16. Magdalena Estirado, E.; Aleman Garcia, M. A.; Schill, J.; Brunsveld, L., Multivalent Ultrasensitive Interfacing of Supramolecular 1D Nanoplatforms. *J Am Chem Soc* **2019,** *141* (45), 18030-18037.
17. Deal, B. R.; Ma, R.; Ma, V. P.; Su, H.; Kindt, J. T.; Salaita, K., Engineering DNA-Functionalized Nanostructures to Bind Nucleic Acid Targets Heteromultivalently with Enhanced Avidity. *J Am Chem Soc* **2020,** *142* (21), 9653-9660.
18. Regan, J. F.; Kamitaki, N.; Legler, T.; Cooper, S.; Klitgord, N.; Karlin-Neumann, G.; Wong, C.; Hodges, S.; Koehler, R.; Tzonev, S.; McCarroll, S. A., A rapid molecular approach for chromosomal phasing. *PLoS One* **2015,** *10* (3), e0118270.
19. Zheng, G. X.; Lau, B. T.; Schnall-Levin, M.; Jarosz, M.; Bell, J. M.; Hindson, C. M.; Kyriazopoulou-Panagiotopoulou, S.; Masquelier, D. A.; Merrill, L.; Terry, J. M.; Mudivarti, P. A.; Wyatt, P. W.; Bharadwaj, R.; Makarewicz, A. J.; Li, Y.; Belgrader, P.; Price, A. D.; Lowe, A. J.; Marks, P.; Vurens, G. M.; Hardenbol, P.; Montesclaros, L.; Luo, M.; Greenfield, L.; Wong, A.; Birch, D. E.; Short, S. W.; Bjornson, K. P.; Patel, P.; Hopmans, E. S.; Wood, C.; Kaur, S.; Lockwood, G. K.; Stafford, D.; Delaney, J. P.; Wu, I.; Ordonez, H. S.; Grimes, S. M.; Greer, S.; Lee, J. Y.; Belhocine, K.; Giorda, K. M.; Heaton, W. H.; McDermott, G. P.; Bent, Z. W.; Meschi, F.; Kondov, N. O.; Wilson, R.; Bernate, J. A.; Gauby, S.; Kindwall, A.; Bermejo, C.; Fehr, A. N.; Chan, A.; Saxonov, S.; Ness, K. D.; Hindson, B. J.; Ji, H. P., Haplotyping germline and cancer genomes with high-throughput linked-read sequencing. *Nat Biotechnol* **2016,** *34* (3), 303-11.
20. Song, T.; Eshra, A.; Shah, S.; Bui, H.; Fu, D.; Yang, M.; Mokhtar, R.; Reif, J., Fast and compact DNA logic circuits based on single-stranded gates using strand-displacing polymerase. *Nat Nanotechnol* **2019,** *14* (11), 1075-1081.
21. Schueder, F.; Lara-Gutierrez, J.; Haas, D.; Beckwith, K. S.; Yin, P.; Ellenberg, J.; Jungmann, R., Super-Resolution Spatial Proximity Detection with Proximity-PAINT. *Angew Chem Int Ed Engl* **2021,** *60* (2), 716-720.
22. Chandrasekaran, A. R.; MacIsaac, M.; Dey, P.; Levchenko, O.; Zhou, L.; Andres, M.; Dey, B. K.; Halvorsen, K., Cellular microRNA detection with miRacles: microRNA- activated conditional looping of engineered switches. *Sci Adv* **2019,** *5* (3), eaau9443.
23. Chen, N.; Schrijver, I., Allelic discrimination of cis-trans relationships by digital polymerase chain reaction: GJB2 (p.V27I/p.E114G) and CFTR (p.R117H/5T). *Genet Med* **2011,** *13* (12), 1025-31.
24. Fan, T. W.; Yu, H. L. L.; Hsing, I. M., Conditional Displacement Hybridization Assay for Multiple SNP Phasing. *Anal Chem* **2017,** *89* (18), 9961-9966.
25. Yu, H. A.; Sima, C. S.; Shen, R.; Kass, S.; Gainor, J.; Shaw, A.; Hames, M.; Iams, W.; Aston, J.; Lovly, C. M.; Horn, L.; Lydon, C.; Oxnard, G. R.; Kris, M. G.; Ladanyi, M.; Riely, G. J., Prognostic impact of KRAS mutation subtypes in 677 patients with metastatic lung adenocarcinomas. *J Thorac Oncol* **2015,** *10* (3), 431-7.
26. Bossert, D.; Urban, D. A.; Maceroni, M.; Ackermann-Hirschi, L.; Haeni, L.; Yajan, P.; Spuch-Calvar, M.; Rothen-Rutishauser, B.; Rodriguez-Lorenzo, L.; Petri-Fink, A.; Schwab, F., A hydrofluoric acid-free method to dissolve and quantify silica nanoparticles in aqueous and solid matrices. *Sci Rep* **2019,** *9* (1), 7938.
27. Mammen, M.; Choi, S. K.; Whitesides, G. M., Polyvalent Interactions in Biological Systems: Implications for Design and Use of Multivalent Ligands and Inhibitors. *Angew Chem Int Ed Engl* **1998,** *37* (20), 2754-2794.
28. Kane, R. S., Thermodynamics of multivalent interactions: influence of the linker. *Langmuir* **2010,** *26* (11), 8636-40.
29. Yakovchuk, P.; Protozanova, E.; Frank-Kamenetskii, M. D., Base-stacking and base-pairing contributions into thermal stability of the DNA double helix. *Nucleic Acids Res* **2006,** *34* (2), 564-74.
30. Lane, M. J.; Paner, T.; Kashin, I.; Faldasz, B. D.; Li, B.; Gallo, F. J.; Benight, A. S., The thermodynamic advantage of DNA oligonucleotide 'stacking hybridization' reactions: energetics of a DNA nick. *Nucleic Acids Res* **1997,** *25* (3), 611-7.
31. Maldonado-Rodriguez, R.; Espinosa-Lara, M.; Loyola-Abitia, P.; Beattie, W. G.; Beattie, K. L., Mutation detection by stacking hybridization on genosensor arrays. *Mol Biotechnol* **1999,** *11* (1), 13-25.

32. Walter, A. E.; Turner, D. H.; Kim, J.; Lyttle, M. H.; Muller, P.; Mathews, D. H.; Zuker, M., Coaxial stacking of helixes enhances binding of oligoribonucleotides and improves predictions of RNA folding. *Proc Natl Acad Sci U S A* **1994,** *91* (20), 9218-22.
33. Munoz-Maldonado, C.; Zimmer, Y.; Medova, M., A Comparative Analysis of Individual RAS Mutations in Cancer Biology. *Front Oncol* **2019,** *9*, 1088.
34. Lee Yu, H. L.; Fan, T. W.; Hsing, I. M., Oligonucleotide hybridization with magnetic separation assay for multiple SNP phasing. *Anal Chim Acta X* **2020,** *5*, 100050.
35. Zhuang, X.; Lee Yu, H. L.; Hsing, I. M., Toehold probe-based interrogation for haplotype phasing of long nucleic acid strands. *Anal Methods* **2020,** *12* (34), 4185-4190.
36. Chang, W.; Liu, W.; Shen, H.; Chen, S.; Liao, P.; Liu, Y., Molecular AND logic gate for multiple single-nucleotide mutations detection based on CRISPR/Cas9n system-trigged signal amplification. *Anal Chim Acta* **2020,** *1112*, 46-53.
37. Gao, Y.; Wolf, L. K.; Georgiadis, R. M., Secondary structure effects on DNA hybridization kinetics: a solution versus surface comparison. *Nucleic Acids Res* **2006,** *34* (11), 3370-7.
38. Bazrafshan, A.; Kyriazi, M. E.; Holt, B. A.; Deng, W.; Piranej, S.; Su, H.; Hu, Y.; El-Sagheer, A. H.; Brown, T.; Kwong, G. A.; Kanaras, A. G.; Salaita, K., DNA Gold Nanoparticle Motors Demonstrate Processive Motion with Bursts of Speed Up to 50 nm Per Second. *ACS Nano* **2021,** *15* (5), 8427-8438.
39. Yehl, K.; Joshi, J. P.; Greene, B. L.; Dyer, R. B.; Nahta, R.; Salaita, K., Catalytic deoxyribozyme-modified nanoparticles for RNAi-independent gene regulation. *ACS Nano* **2012,** *6* (10), 9150-7.
40. Huskens, J.; Mulder, A.; Auletta, T.; Nijhuis, C. A.; Ludden, M. J.; Reinhoudt, D. N., A model for describing the thermodynamics of multivalent host-guest interactions at interfaces. *J Am Chem Soc* **2004,** *126* (21), 6784-97.
41. Karadeema, R. J.; Stancescu, M.; Steidl, T. P.; Bertot, S. C.; Kolpashchikov, D. M., The owl sensor: a 'fragile' DNA nanostructure for the analysis of single nucleotide variations. *Nanoscale* **2018,** *10* (21), 10116-10122.
42. Zhou, L.; Hayden, A.; Chandrasekaran, A. R.; Vilcapoma, J.; Cavaliere, C.; Dey, P.; Mao, S.; Sheng, J.; Dey, B. K.; Rangan, P.; Halvorsen, K., Sequence-selective purification of biological RNAs using DNA nanoswitches. *Cell Rep Methods* **2021,** *1* (8).